Extraction and Classification of Road Markings Using Mobile Laser Scanning Point Clouds

Ming Cheng, *Member, IEEE*, Haocheng Zhang, Cheng Wang, *Senior Member, IEEE*, and Jonathan Li, *Senior Member, IEEE*

***Abstract*—This study aims at building a robust method for semiautomated information extraction of pavement markings detected from mobile laser scanning (MLS) point clouds. The proposed workflow consists of three components: 1) preprocessing, 2) extraction, and 3) classification. In preprocessing, the three-dimensional (3-D) MLS point clouds are converted into radiometrically corrected and enhanced two-dimensional (2-D) intensity imagery of the road surface. Then, the pavement markings are automatically extracted with the intensity using a set of algorithms, including Otsu's thresholding, neighbor-counting filtering, and region growing. Finally, the extracted pavement markings are classified with the geometric parameters by using a manually defined decision tree. A study was conducted by using the MLS dataset acquired in Xiamen, Fujian, China. The results demonstrated that the proposed workflow and method can achieve 92% in completeness, 95% in correctness, and 94% in *F*-score.**

***Index Terms*—Decision tree, mobile laser scanning (MLS), point cloud, region growing, road marking.**

I. Introduction

DRIVERLESS car is one of the focus areas of current research on intelligent transportation systems. As a robotic vehicle that is capable of traveling between destinations without a human operator, the driverless car is driven not by human but the data. There are two principal data sources for the navigation of driverless cars. The first one is the sensory input in terms of the surroundings of the driverless car, collected by the radar, light detection and ranging (LiDAR), video cameras, etc. The second one is a prior highly detailed three-dimensional (3-D) map. The highly precise map is indispensable not only to allow a car to locate itself on the traffic lane, but also to enable a vehicle to take corresponding actions correctly [1]. In a scenario where a driverless car tries to overtake a slower truck in front of it on a freeway, the car itself must have the knowledge that there is another lane to move into. The width of the lane and the stretch length of the road for completing the maneuver also need to be taken into consideration. Thus, the automated car has to be supported by a detailed lane model. Such a lane model needs to have precise lane geometry with lane boundaries and rich attributions such as lane types, lane traversal information, lane marking types, and lane speed limit information [2].

To capture the world in 3-D for autonomous vehicles, mobile laser scanning (MLS) technology is applied before the driverless cars hit the road. It is an effective and efficient method for acquiring highly accurate, precise, and dense georeferencing 3-D topographic data [3]. MLS systems are the mobile mapping systems based on the LiDAR, which capture 3-D point clouds from the surrounding environment by using profiling scanners. Compared to camera sensors, MLS is less sensitive to weather and sunlight, and the result retrieved from the MLS-based extraction is more comprehensive and accurate than the one obtained from the image- or video-based extraction method. Thus, MLS is more suitable for surveying and mapping application [4], [5] where georeferencing data are indispensable.

It is noted that the majority of the information of lanes is represented by the road markings, and the main purpose of this study is to develop a semiautomatic workflow for road-marking detection and classification by using 3-D point clouds acquired by a vehicle-mounted MLS system. The positioned and recognized road markings can be transformed into lane information to support the operation of the driverless car.

In order to extract the road markings efficiently, the first step is to extract the road surface from the large-volume raw MLS data. A variety of methods were developed to detect roads from point clouds, which can be classified into four categories: 1) scan line segmentation, 2) planar surface extraction, 3) 3-D geometric features filtering, and 4) voxel-based algorithm.

The scan-line-based segmentation splits the MLS data into scan lines (profiles), and then focuses on the detection of the road edges or curbs based on the elevation changes in each scan line. A rapid change of slope is employed to distinguish a curb or road border from the ground [6]–[9]. Different from road edge detection, planar surface extraction aims at extracting the road surface directly according to its smoothness. It takes the coplanarity and connectivity into consideration and detects the road

Manuscript received May 18, 2016; revised August 14, 2016; accepted September 2, 2016. Date of publication September 27, 2016; date of current version February 13, 2017. This work was supported in part by the National Natural Science Foundation of China under Grant 41471379 and Grant 61371144, and in part by the Fujian Collaborative Innovation Center for Big Data Applications in Governments. *(Corresponding author: Jonathan Li.)*

M. Cheng and C. Wang are with the Fujian Key Laboratory of Sensing and Computing for Smart Cities, School of Information Science and Engineering, Xiamen University, Xiamen 361005, China (e-mail: chm99@xmu.edu.cn; cwang@xmu.edu.cn).

H. Zhang is with the Department of Geography and Environmental Management, University of Waterloo, Waterloo, ON N2L 3G1, Canada (e-mail: h232zhan@uwaterloo.ca).

J. Li is with the Fujian Key Laboratory of Sensing and Computing for Smart Cities, School of Information Science and Engineering, Xiamen University, Xiamen 361005, China, and also with the Department of Geography and Environmental Management, University of Waterloo, Waterloo, ON N2L 3G1, Canada (e-mail: junli@uwaterloo.ca).

Color versions of one or more of the figures in this paper are available online at http://ieeexplore.ieee.org.

Digital Object Identifier 10.1109/JSTARS.2016.2606507

surface in a global scale [10]–[12]. In a rough classification, the road surface segments could be extracted based on the distance to the vehicle trajectory. In the third category, the road surface is also extracted in a global scale by a 3-D features filtering, such as normal vector [13], and slope and height variance [14]. A voxel-based algorithm utilizes the connectivity along the vertical direction, and elevation threshold is used to separate ground from nonground points [15], [16].

A variety of studies have been reported on road-marking extraction and classification from the MLS data. In general, the road markings have much higher reflectance than the unpainted road surface. Therefore, the relatively high intensity can be used for detecting the road markings. However, some factors would impact the intensity data measured by MLS systems, such as scan range, incidence angle, and surface properties.

According to the approach to solve the "inconstant intensity" issue, the extraction process can be classified into three categories: 1) global intensity filtering, 2) global intensity filtering with preprocessing, and 3) multithresholding segmentation.

With regard to global intensity filtering, Smadja *et al.* [17] implemented a simple threshold on intensity for detecting the road markings. Toth *et al.* [18] selected an intensity value based on the intensity distribution in a search window as a global threshold for the extraction. In [19], a two-step filtering was undertaken for MLS point clouds based on intensity and elevation information, and then the markings were detected according to their patterns and arrangements.

To eliminate the intensity variance caused by the unevenly distributed point clouds, Jaakkola *et al.* [20] applied a preprocessing step to correct the intensity data before extraction. They projected the MLS point clouds onto raster images, and used image processing algorithms to extract markings. First of all, the intensity image was profiled by column in the study. Along the profile, a second-order curve fitted the median intensity measurements to reduce the variance of the measured intensity value. After radiometric correction, a 3×5 average filter was applied for denoising the corrected image. Then a constant threshold was used to extract road markings.

It is noted that the inconstancy of the intensity value may result in errors in the extraction results. Therefore, multithresholding segmentation was employed to minimize the impact of the inconsistent intensity [7], [21]–[24]. Chen *et al.* [21] selected the intensity peaks along the scan line as lane marking points by using adaptive thresholding. Vosselman [22] proposed a distance-dependent thresholding method to detect the road markings, and a connected components analysis to extract road markings. Kumar *et al.* [23] applied a range-dependent thresholding function to extract road markings from intensity and range images. The algorithm proposed in [21] is a transversal segmentation, whereas the methods used in [22] and [23] are a longitudinal segmentation.

In other studies, the distance-dependence of intensity was used in different ways. Guan *et al.* [7] implemented point-density-dependent multithresholding segmentation to extract road markings. The distribution of point density along the cross section was fitted to a Gaussian normal distribution function. The road surface points were segmented into some bins according to the range that was calculated by the estimated mean and standard deviation. Yu *et al.* [24] applied a distance-dependent multithresholding segmentation in which the road surface points were segmented into the blocks along the road. A distance-based segmentation was then used to partition the blocks into segments, in which each segment was threshold by Otsu's method individually.

Based on the findings from the literature review, the majority of the research did not undertake radiometric correction for reducing intensity variance before road-marking extraction, except the work in [20]. Thus, this study aims at introducing an improved radiometric correction of laser intensity for road-marking extraction to improve the road-marking-extraction result.

The classification of road markings commonly consists of three steps: 1) splitting road markings into objects, 2) extracting features of objects, and 3) recognizing road-marking objects. The first stage is to segment the whole road markings into portions for recognition. The road-marking segmentation can be classified into three categories: 1) the Hough transform [21], [25], [26]; 2) the contour-based analysis [27]; and 3) the region-based analysis [24], [28], [29].

Feature extraction retrieves the shape information to facilitate the shape recognition. It should be noted that the majority of the road markings are line-shaped or rectangular; therefore, only a few of the shaped-based extraction techniques were used in road-marking-recognition studies. Rebut *et al.* [26] used a 1-D Fourier descriptor as the shape signatures for the recognition of the road arrows. In [27], many features of simplified contours were calculated for classification, including the aspect ratio of the glyph, normalized central moment, horizontal/vertical projection of the glyph, and fuzzy zoning of angles. Franke *et al.* [28] computed the area, bounding box, aspect ratio, length, and smoothness of contour for road-marking recognition. Foucher *et al.* [29] calculated the minimum bounding box of connected components in an image and then classified the components into crosswalks and arrows by their areas, rectangularity, and profiles. Li *et al.* [30] identified arrow markings based on the shape information, such as chain code, moment features, length, and aspect ratio of a minimum bounding box. Tournaire *et al.* [31] used various variables (i.e., centroid and orientation, width, and length) to describe rectangular marking, and used a wavelet feature to describe arrow markings. Danescu and Nedevschi [32] applied random sample consensus to extract the edge lines of the road markings, and then defined three characteristics from the edge lines. Wu and Ranganathan [33] detected corners in road-marking regions, labeled the corners as the points of interest (POI), and then calculated the histogram of oriented gradients (HOG) of each POI as the features of the shape.

A number of supervised classification methods were developed for recognizing road markings. In [32], the road markings were classified by defining a decision tree based on the shape of the road markings. Based on the Euclidean distance clustering result of road-marking points, Yu *et al.* [24] trained the deep Boltzmann machine model with 2-D images of small-sized road markings, and the small-sized road markings were then classified into different categories (i.e., arrow markings, rectangular-shaped marking, pedestrian warning marking, and other markings). Sample glyphs were manually extracted from

real road footage sequences in [27] and an artificial neural network classifier was trained for recognizing road markings. Li *et al.* [30] generated a Bayes classifier with minimum error rate training in which over 5000 samples of five different road markings were used to train the classifier. Wu and Ranganathan [33] generated the feature vectors from HOG for each POI in all template images, and then road markings were identified by the template matching method. Wang *et al.* [34] designed a multiclass support vector machine (SVM) to classify arrow markings based on the hierarchical classification method. The SVM classifiers at the nodes of the hierarchical tree were trained to form the hierarchical classification. Mathibela *et al.* [35] classified the road markings into seven distinct classes within a conditional random field and probabilistic RUSBoost classification framework by employing a set of geometric feature functions.

It was identified from the review that machine learning algorithms were widely used for road-marking recognition, except the study conducted by Danescu and Nedevschi [32], in which rules were encoded in a simple decision tree to classify the road markings. It is noted that the machine learning algorithms require training of the samples to determine whether a candidate matches a model sufficiently. In addition, the success of the road-marking classifications relies on the quality and quantity of the training dataset. There was a positive correlation between the number of the training samples and the performance of the machine learning algorithms. On the other hand, manually building the decision tree relies on the strong prior knowledge. It is clear that the pavement marking guide, as strong prior knowledge, can be easily encoded in the decision tree as rules, whereas the machine learning algorithms need training process.

The main novelties of this work are as follows: A hybrid road-surface extraction method was developed for road surface detection, the scan-angle-rank-based intensity correction was undertaken to attenuate the intensity variance caused by varying incidence angles, the large-size high-pass filter was utilized to attenuate the intensity variance caused by different degrees of surface roughness, and a shape-based hierarchical tree for road-marking classification was defined based on the comprehensive prior knowledge of the road-marking shapes.

The rest of this paper is organized as follows. Section II gives a brief introduction of the survey area and dataset in this study. Section III describes the proposed road-marking extraction and classification method. Section IV reports and discusses the experimental results. Concluding remarks are given in Section V.

II. Study Area and Dataset

The area selected in this study is located in Xiamen, China (see Fig. 1). An MLS survey was carried out back and forth on Xiamen Island Ring Road on April 23, 2012, by using a RIEGL VMX-450 system. The Ring Road is a two-side, four-lane road with a center median. The total length of the survey in one direction was around 10 km. The majority of the road surface and road markings are in good condition. Seven samples of the survey data (i.e., the straight and curve roads, and different types of road markings) were selected as the test dataset for evaluating the proposed method. The average point density of the dataset is 7 000 points/m^2. The dataset was then converted into the format of LAS, which is a standard in the laser scanning industry.

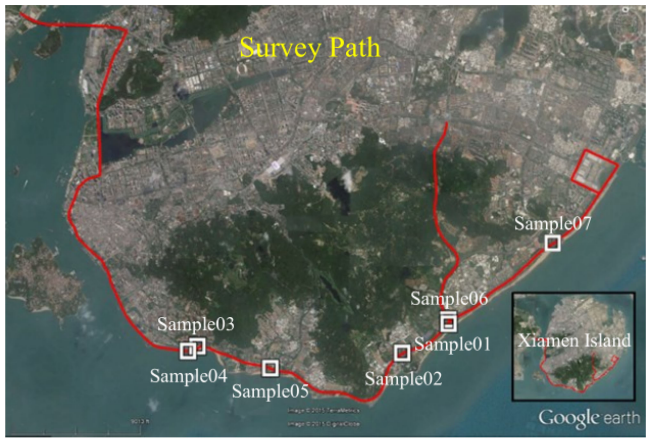

(a)

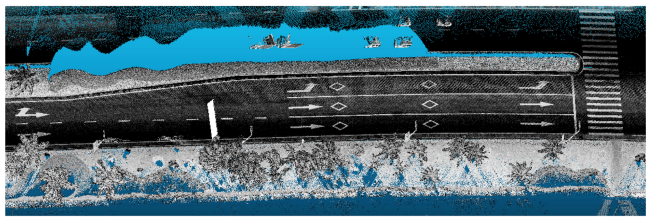

(b)

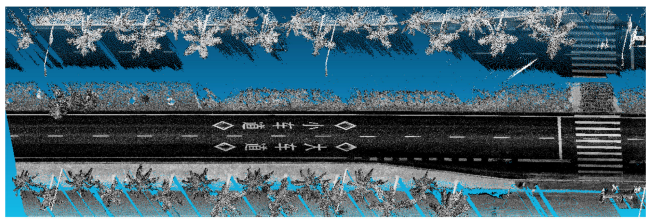

(c)

Fig. 1. (a) Study area: Island Ring Road in Xiamen, Fujian, China, and (b) and (c) 3-D point cloud intensity images of Sample01 and Sample 05, respectively.

III. Methods

The proposed method in this study consists of three phases, including preprocessing, road-marking extraction, and road-marking classification.

A. Preprocessing of MLS Data

The raw point clouds are preprocessed in two steps to reduce the volume of the data and overcome the problem resulting from the uneven distribution of intensity. The workflow is shown in Fig. 2.

1) Road Surface Extraction: The raw MLS data include various nonground points, such as the pedestrians, vehicles, trees, poles, and buildings. In order to eliminate the disturbance from nonroad points and improve the computational efficiency, these nonroad points are removed prior to the extraction. A hybrid road surface extraction is introduced in this step, including a

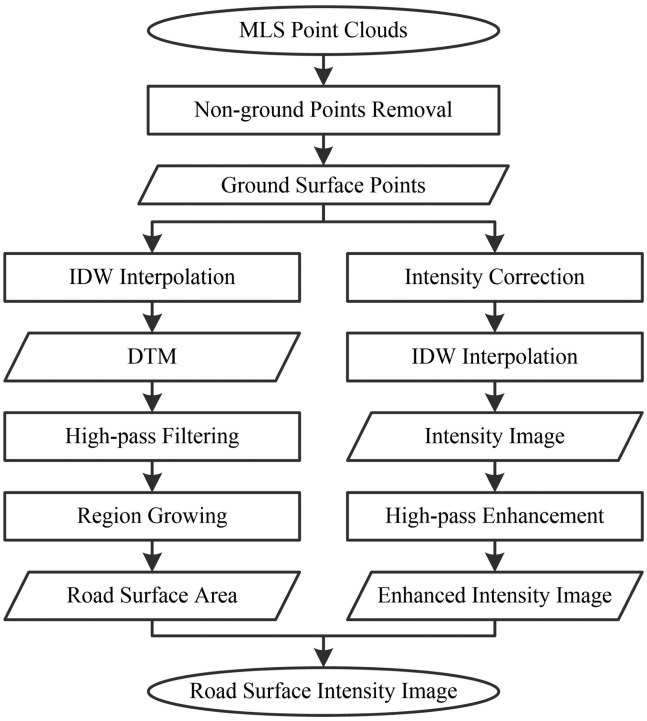

Fig. 2. Workflow of preprocessing.

voxel-based upward growing, digital terrain model (DTM) interpolation, high-pass filtering, and region growing segmentation.

A voxel-based upward growing method [16] is employed to segment the raw MLS data into ground points and nonground points. This method partitions point cloud data into an octree structure with a voxel size. For each voxel, it expands to its nine-neighbor upward voxels, and then the growing scheme expands until it reaches the top boundary. If the elevation of the top voxel is smaller than the predefined threshold, the cluster of these voxels is referred to the ground. The point clouds in these voxels are labeled ground points. Otherwise, the point clouds will be categorized as nonground points.

In the removal process, all the nonground points are removed from raw point clouds. The ground points are then rasterized into the DTM by inverse distance weighting (IDW) interpolation. With the IDW interpolation, the gray value of a grid is interpolated with its neighbors:

$$z = \sum_{k=1}^{n} w_k z_k \Big/ \sum_{k=1}^{n} w_k \tag{1}$$

where $w_k = 1/d_k^2$ is the weight of the kth point within the grid, as a function of distance d_k, z_k is the kth point gray value that can either be an elevation value or intensity value, and n is the number of points in a grid. When z_k represents the elevation of the point, the result of the IDW interpolation is the DTM; when z_k represents the intensity of the point, the result is an intensity image of the ground.

The main features of the road surface are characterized by its smoothness and connectedness. In general, the surface of the grass is rougher than the road surface. Additionally, it is clear that the existence of a curb would result in a sudden change in the height of the road boundary. Therefore, a high-pass filter is applied to the DTM. The absolute value of the filtering result indicates the roughness of the surface. A 3×3 high-pass kernel and a 5×5 high-pass kernel are shown in Fig. 3. To distinguish the road surface from other grounds (e.g., lawn and curbs), a threshold should be defined based on the absolute value of the filter results. The pixels under the threshold are clustered by region growing, among which the largest region is a road surface.

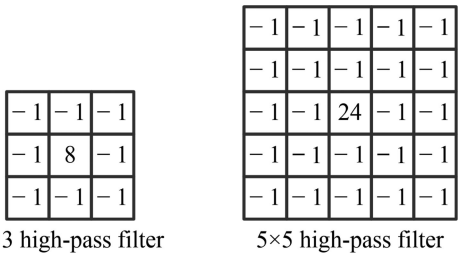

Fig. 3. High-pass filter kernels.

2) Intensity Image Generation and Refinement: The points of the road surface are rasterized into a 2-D intensity image by using IDW interpolation. Although the elevation information is lost after the dimensionality reduction, the intensity information is retained in the 2-D image, which is essential for the road-marking extraction.

Road markings are highly reflective materials painted on road surfaces; therefore, they show higher intensities than their surrounding road surface in the point cloud. However, the reflected laser light intensities are affected by various factors. A laser light follows the reflection and transmission of electromagnetic radiation. The strength of its intensity measured by a scanner depends on the range from the laser point to the scanner, the incidence angle of a laser beam, and the material property. Generally, the reflected laser light intensity decreases with increase of incident angles and ranges. As a result, the road markings farther away from the scanner center exhibit relatively lower intensities than those of the road markings nearer to the scanner center. Therefore, the intensities of road markings distribute unevenly and fluctuate strongly in the road surface point cloud [24].

The unevenly distributed intensity leads to a large in-class variance of road-marking points, which affects the extraction of the road markings. A variety of methods were developed to overcome the distribution issue of MLS data. For example, the MLS dataset can be partitioned into subsets, such as segments or profiles, to reduce the in-class variance and improve the extraction performance. In this study, a scan-angle-based intensity correction was adopted to reduce the variance of intensity directly.

The strength of point intensity depends on the range from the laser point to the scanner, the incidence angle of a laser beam, and the material property. The height of the scanner is constant during the survey since it is mounted on a vehicle; then the range is a function of the incidence angle. Furthermore, for road-marking extraction, the material property of markings is the same. Thus, the point intensity is a function of the incidence angle. An empirical correction function was introduced to use

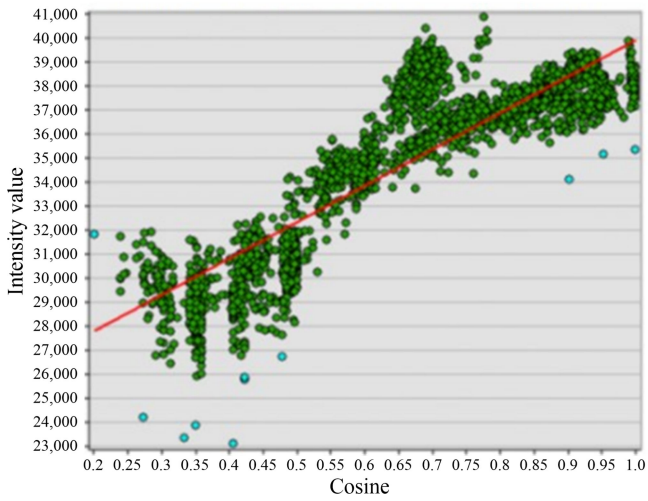

Fig. 4. Intensity of pure road-marking points versus cosine of the scan angle rank (from Sample05). Green points are the inlier and cyan points are the outlier. The red line is the trend of the linear regression.

an incidence angle to express received intensity [36]:

$$I(\theta) = a_{\omega,g}(1 - b_{\omega,g}(1 - \cos\theta)) \tag{2}$$

where θ represents the incidence angle, ω is the reflectance or albedo, and g is the grain size of the material. In the case that the material property of marking is the same, the albedo ω and grain size g are constant, and $a_{\omega,g}$ and $b_{\omega,g}$ are constant too. As a result, (2) can be simplified as follows:

$$I(\theta) = A\cos\theta + B \tag{3}$$

where A and B are the constants that depend on the albedo and grain size of the material. Therefore, the intensity value received by the scanner can be corrected with incidence angle θ. However, an accurate incidence angle can be calculated by using only the direction of the laser beam and normal vector of the surface, which is time-consuming with massive calculations. A simple and rough way is to employ the scan angle rank recorded in MLS data as an estimator. The absolute value of the scan angle rank is close to incidence angle when the ground surface is planar. The relationship between the marking point intensity and the cosine of the scan angle rank is shown in Fig. 4. After the removal of the outlier, a linear regression model is derived between the intensity and the cosine as

$$I(\theta) = 15115\cdot\cos\theta + 24794. \tag{4}$$

In this model, the *R*-squared is 0.77, and the *P*-value is less than 0.0001. It indicates that the model can explain 77% variance of the road-marking pixel intensity, and the correlation between the cosine of scan angle and the intensity value is significant. With this linear regression model, the road-marking intensity can be corrected and the majority of the in-class variance of the road marking intensity will be eliminated.

Because the pavement surface is polished by road traffic, the point clouds of pavements would have various intensity values. The intensity correction based on (4) is not able to eliminate the variance of intensity caused by different degrees of roughness of pavements. A large-size high-pass enhancement is utilized on the corrected intensity image to eliminate the slowly varying intensity components. The kernel of the filter has to meet the requirements as follows. First, the kernel size must be large enough to contain both road-marking pixels and pavement pixels. Second, the kernel size should be small enough to avoid the impact of the spatial variance of the intensity. The best kernel size and the performance of the high-pass filter enhancement will be discussed in Section IV.

B. Extraction of Road Marking

Otsu's thresholding method is applied to extract road markings based on the discriminant analysis. It is assumed that the image is bimodal and the illumination is uniform; therefore, the bimodal brightness can be determined based on the differences of the materials' properties. The road surface area is preserved in the intensity images in the format of either the asphalt pavements or the road markings. With the assistance of the intensity correction and enhancement, the illumination in the image is uniform. Thus, the enhanced and corrected intensity image is able to meet the requirements of Otsu's thresholding method.

Let T be an intensity threshold that separates the road surface intensity image into road markings (greater than T) and pavements (smaller than T), ω_M and ω_P be the proportions of marking pixels and pavement pixels with respect to the whole image, where $\omega_M + \omega_P = 1$, and let μ_M and μ_P be the mean intensity values of the two classes. The mean intensity value of the whole image is

$$\mu = \omega_M\mu_M + \omega_P\mu_P.$$

The interclass variance is defined as

$$\begin{aligned}\sigma^2(T) &= \omega_M(\mu_M - \mu)^2 + \omega_P(\mu_P - \mu)^2 \\ &= \omega_M\omega_P(\mu_M - \mu_P)^2\end{aligned} \tag{5}$$

which is a function of T. Otsu's thresholding determines the optimal threshold T^* by maximizing the interclass variance as

$$T^* = \arg\max\sigma^2(T). \tag{6}$$

The scan-angle-rank-based intensity correction is capable of eliminating only the intensity variance for a flat road surface. In the surveying of a poor-conditioned road, the laser beam may scan at the crack or the rutting slope. The relatively smaller incidence angle of the cracks and rutting would result in a brighter intensity compared to their neighboring road surface and cause a false positive in the thresholding result. Another false positive could be resulted from the boundary of two different pavements, which is enhanced by the high-pass enhancement. Two denoising methods are employed, including median filtering and region growing segmentation [37]. Small pixels of false positive and false negative (pepper noise) can be eliminated by using the median filtering approach. The segments of false positive with medium sizes (e.g., small fragments of cracks and manholes) can be removed by using the region growing segmentation if they are smaller than the smallest road-marking segment.

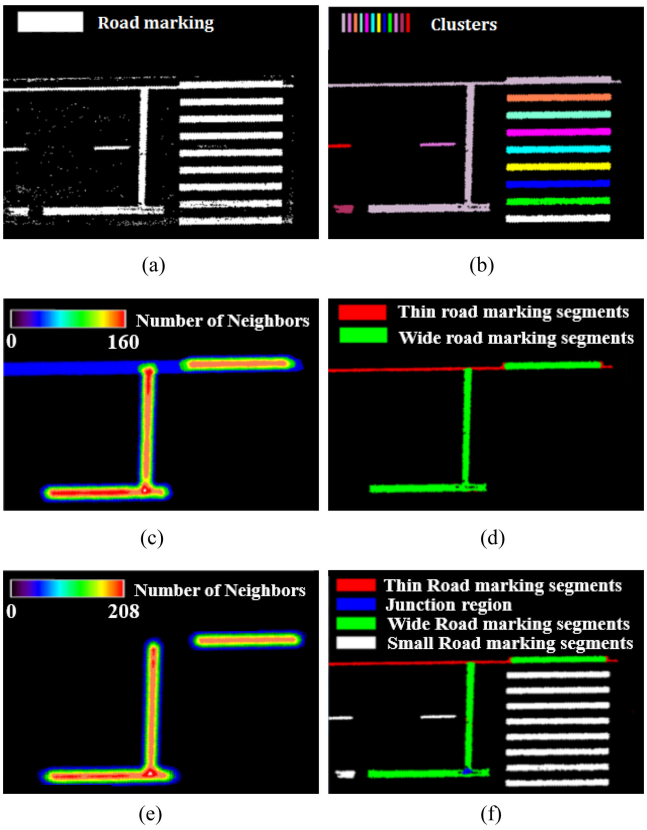

Fig. 5. Road-marking segmentation: (a) thresholding result, (b) region growing result, (c) neighbor-counting image of large segment, (d) thin and wide road-marking segments, (e) junction detection based on neighbor counting, and (f) segmentation result.

C. Classification of Road Marking

The road-marking classification consists of three steps, including road-marking segmentation, feature extraction, and road-marking classification.

1) Road-Marking Segmentation: The first step of road-marking classification is dividing the extracted road marking into segments, where a four-neighbor region growing segmentation is employed. The region growing has the capacity of separating different clusters and ensures the connection of the pixels in each cluster. After region growing, regions smaller than the smallest road marking are removed from the road-marking segments.

The road markings attached to each other could be merged into a large region [see Fig. 5(b)]. This large road marking should be segmented into a few road markings to guarantee the subsequent recognition of transverse road-marking and zebra-crossing stripes. Taking the width and junction into consideration, the large road marking can be easily classified into two types: 1) the thin road marking and 2) the wide road marking. The segmentation method consists of two steps: 1) distinguishing thin and wide road markings, and 2) splitting road markings at junctions. The neighbor-counting filtering is applied to detect the thin, wide road markings and their junctions.

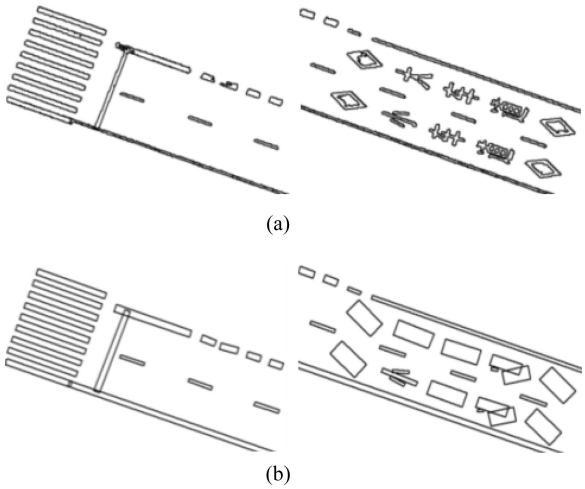

Fig. 6. (a) Boundaries of road-marking segments and (b) bounding rectangles of road-marking segments.

The width of road markings can be inferred by counting the neighbors of a pixel. As shown in Fig. 5(c), in terms of the road-marking pixels, the wide road-marking pixels have more neighbors, whereas the thin markings have fewer. Therefore, wide markings and thin markings can be distinguished, as illustrated in Fig. 5(d). Fig. 5(e) shows the neighbor counting of wide markings. It can be observed that junction regions have more neighbors; thus, junctions can be detected by the application of the neighbor-based filtering. The final segmentation result is presented in Fig. 5(f).

2) Feature Extraction: After the road marking is partitioned into segments, geometric parameters of marking segments are calculated. Four parameters are employed in road-marking classification, including area, perimeter, estimated width, and orientation. Area and perimeter, as the basic geometric parameters of a road marking, can be directly calculated. The estimated width is defined as

$$\text{Estimated width} = \frac{2 \times \text{Area}}{\text{Perimeter}}. \tag{7}$$

Although this estimated value is not the true width of the segment, it can indicate the thinness of road markings. Based on the area and width of the road marking, rectangular markings can be detected and recognized, but irregular markings having a similar area and width may be misclassified. In this case, a minimum bounding rectangle (MBR) is derived to present the extent of each road marking (see Fig. 6). According to the width of MBRs, road markings can be classified into the road marking in thin MBRs (e.g., zebra strip and dashed line) and road marking in wide MBRs (arrow, diamond, character, and number). Based on the MBRs, the main angle of a road marking can be calculated. Compared with longitudinal markings, transverse markings have a higher variance of the main angle in a section of the road. It makes transverse markings distinguishable from longitudinal markings.

Compared to other shape descriptors, area, perimeter, and estimated width require relatively low computational work.

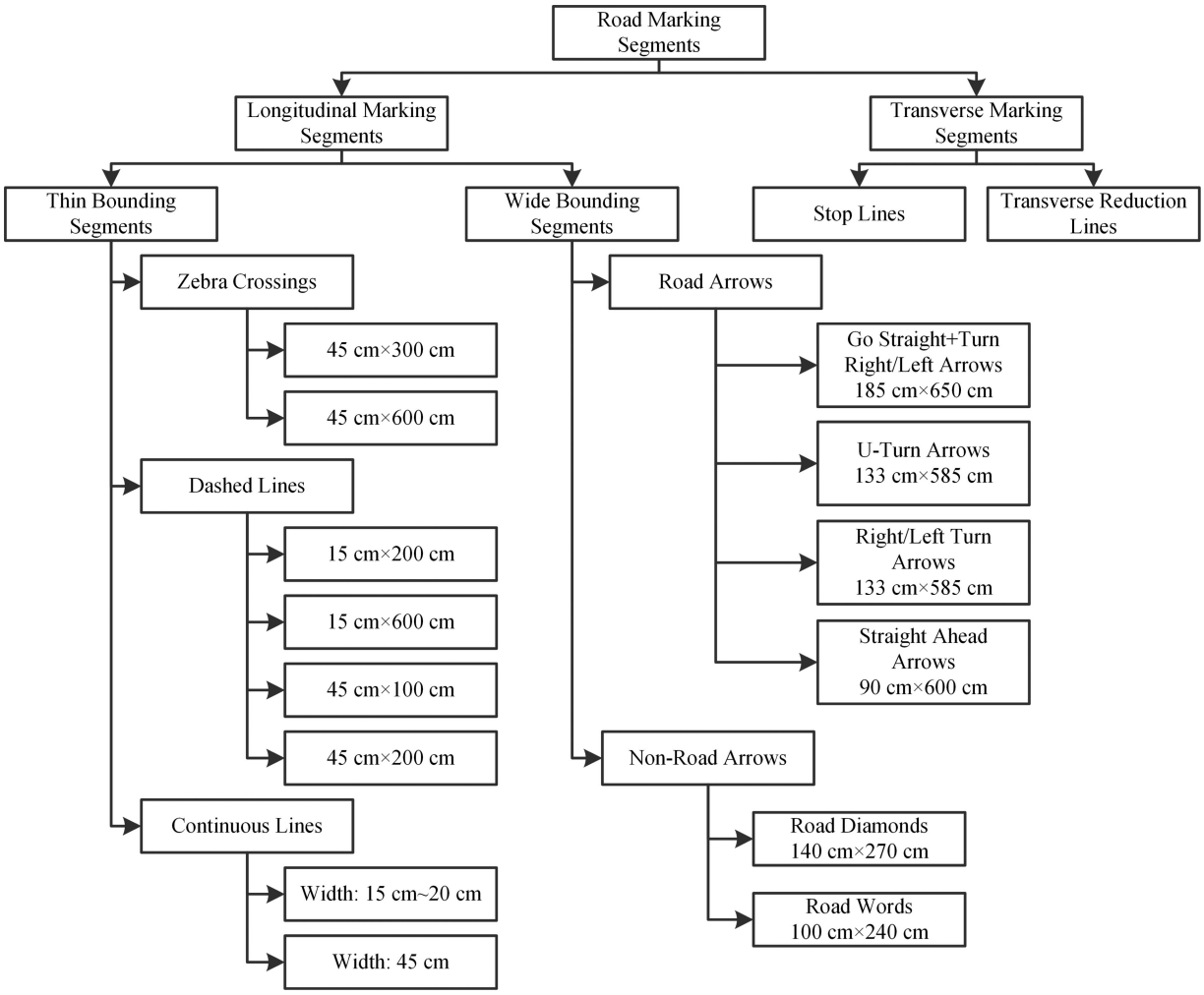

Fig. 7. Hierarchical tree of the road-marking categories.

They can be calculated more rapidly than other advanced shape descriptors, such as moment, chain code, profiles, Fourier descriptor, and wavelet transform. Thus, in this study, these three basic shape parameters are used to describe the shape of road markings for further recognition. The MBR and its orientation are then employed to make the different road markings more distinguishable and recognizable from others.

3) Road-Marking Classification: Based on strong prior knowledge of the road-marking criteria, road-marking segments can be grouped into classes based on their geometric features. A decision tree is designed and developed for the classification. The hierarchical tree of road-marking categories developed in this study is illustrated in Fig. 7. According to the People's Republic of China National Standards: Road Traffic Marking (2009), the road markings in the Xiamen dataset can be classified into two categories: 1) longitudinal marking and 2) transverse marking. The orientation of road-marking segments can be measured by the main angle of MBRs. Transverse and longitudinal markings have a high and low variance of the main angle in a section of the road, respectively. The difference of orientation variance is adopted as the rule for the first level of the decision tree. Transverse markings of the Xiamen dataset include stop lines and transverse reduction lines. At the second level, longitudinal marking segments are separated into two groups based on the MBR width. In the third level, if the width of the segment exceeds 45 cm, it is referred to as a wide MBR (i.e., road arrow or nonroad arrow); otherwise, it is referred to as a thin MBR (i.e., strip of zebra crossing, dashed line, or continuous line). In the fourth level, zebra crossings, dashed lines, continuous lines, road arrows, and nonroad arrows are further classified into specific subclasses based on their area and estimated width.

The classification result is illustrated in Fig. 8. At the first level, the marking segments are categorized into transverse markings (red) and longitudinal markings (white). At the second level, the longitudinal markings are divided into thin MBRs (white) and wide MBRs (blue). Fig. 8(c) shows the subclasses of thin MBRs, including zebra crossings (purple), dashed lines (green), and continuous lines (yellow). At the fourth level, the categories of the road markings are subclassified into specific types (e.g., 15 cm $\times$ 200 cm dashed line and 45 cm $\times$ 100 cm dashed line).

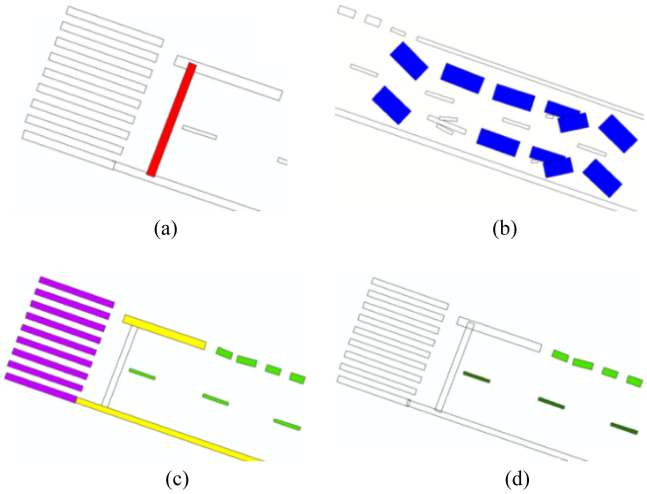

Fig. 8. Decision-tree classification. (a)–(d) Results of levels 1–4.

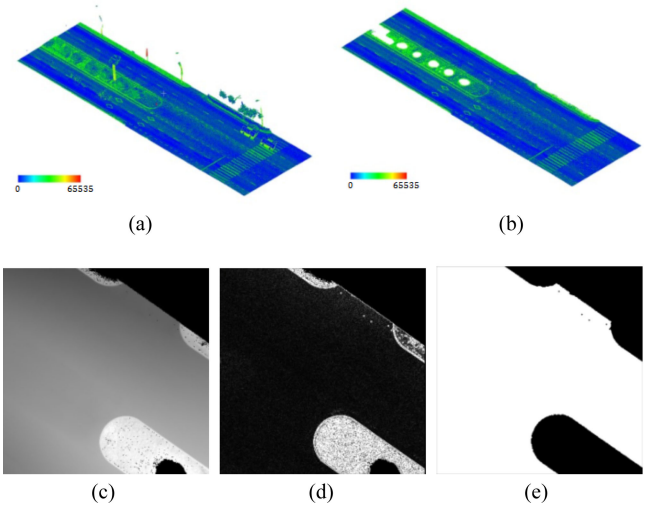

Fig. 9. (a) Raw data from Sample07, (b) ground surface points, (c) DTM (5 cm grid size), (d) high-pass filtering result, and (e) thresholding and region growing results.

IV. Results and Discussion

In this section, the results of each step of the proposed method are given, and the optimal values of some parameters, e.g., the grid size of DTM and the kernel size of high-pass filter, are discussed. The following three measures are used to evaluate the results of road-marking extraction in the comparative study [7]:

$$\text{Completeness} = \frac{\text{TP}}{\text{TP} + \text{FN}} \tag{8}$$

$$\text{Correctness} = \frac{\text{TP}}{\text{TP} + \text{FP}} \tag{9}$$

$$F\text{-score} = \frac{2 \times \text{Completeness} \times \text{Correctness}}{\text{Completeness} + \text{Correctness}} \tag{10}$$

where TP, FN, and FP are the numbers of true positive, false negative, and false positive, respectively.

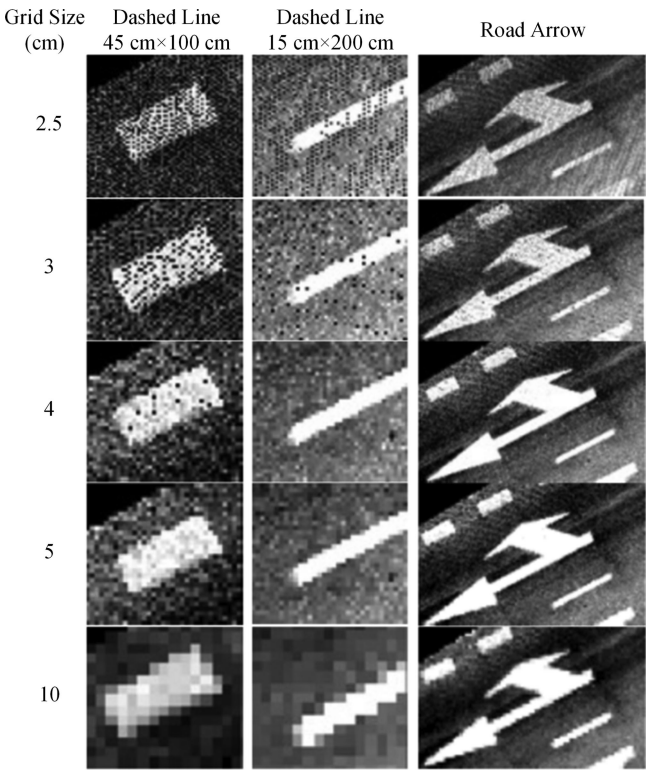

Fig. 10. Intensity image generated at different resolutions.

A. Road Surface Extraction

Voxel-based upward growing was used to remove the non-ground points from the MLS dataset. Fig. 9(a) and (b) presents the raw MLS data of Sample07 and its ground surface points with intensity value, respectively. The road surface region was extracted by the integration of IDW interpolation, high-pass filtering, thresholding, and region growing segmentation. Fig. 9(c) provides a view of the DTM created from ground surface points, where the black area represents no-data area. The grid size of the DTM was set to 5 cm. The large gray area refers to the road surface and the brighter regions represent the median strips. The 3×3 high-pass filtering result of the DTM is shown in Fig. 9(d). It is noted that the high-pass result of the road surface is much lower than that of the other surfaces. With a defined threshold (0.04 m in this dataset, determined by manual selection), the objects (e.g., grass and curbs) can be distinguished from the ground. Due to the character of continuous connectivity, the road surface is obtained as the largest smooth region, as shown in white in Fig. 9(e).

B. Intensity Image Generation and Refinement

The IDW interpolation was applied to the intensity values of the ground surface points derived from MLS data at different levels. The high resolution can result in the increased volume of data and workload for computation. From a grid size of 2.5 to 10 cm, the intensity images of the road markings were blurred and the computational work was decreased (see Fig. 10). With a

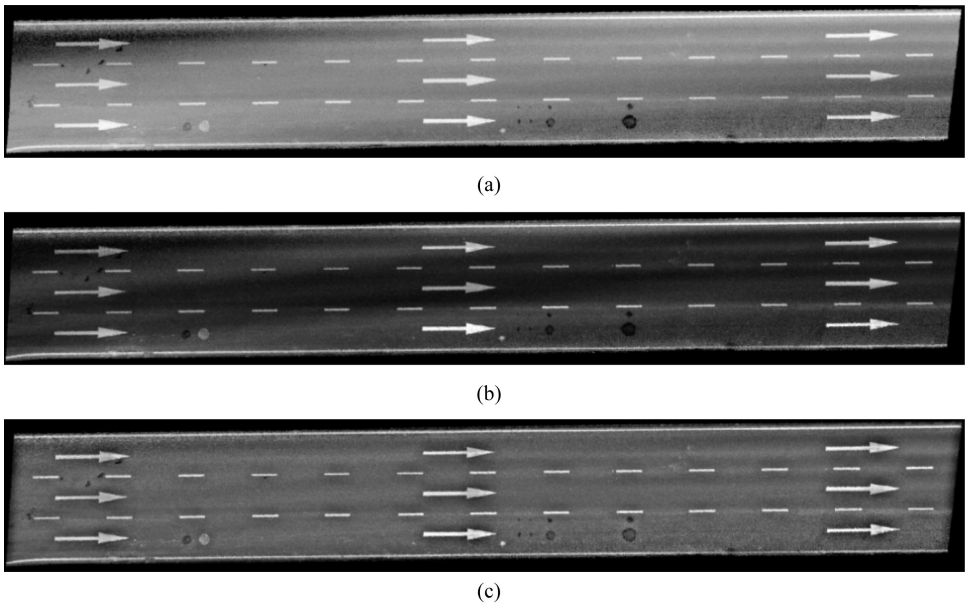

Fig. 11. Intensity image of Sample06. (a) IDW interpolation result, (b) scan-angle-rank-based intensity correction result, and (c) high-pass filtering result.

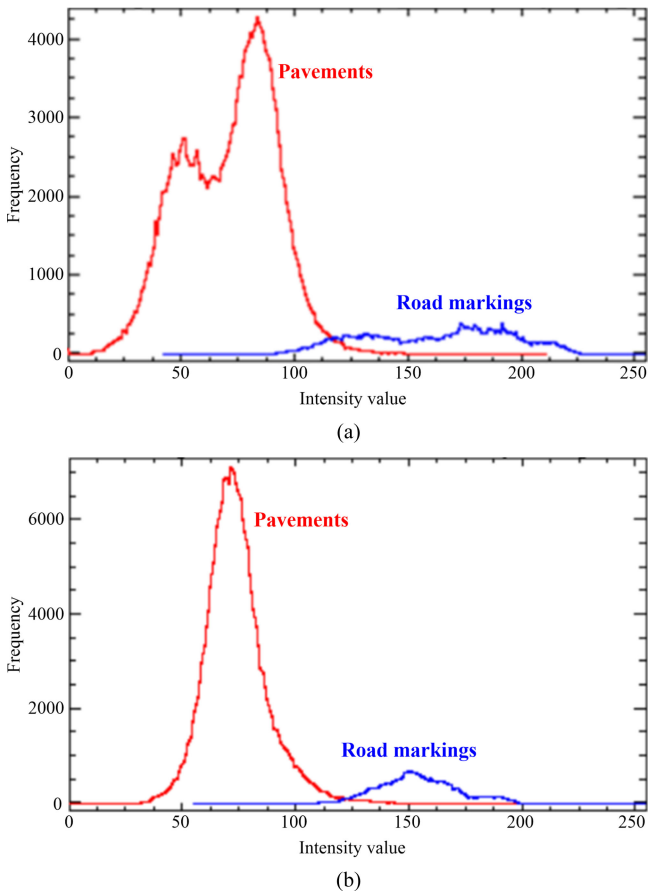

Fig. 12. Histograms of the road markings and pavements. (a) Before correction and (b) after correction.

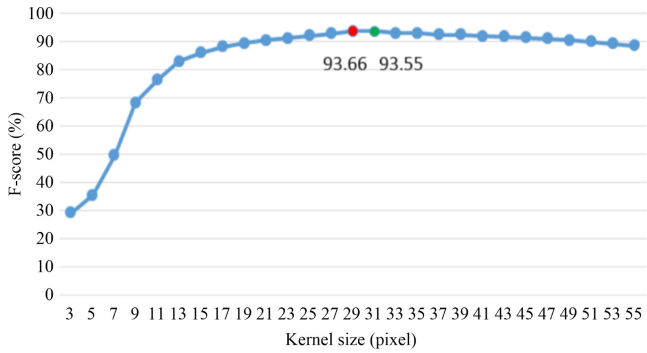

Fig. 13. Performance of different high-pass filters with Sample06.

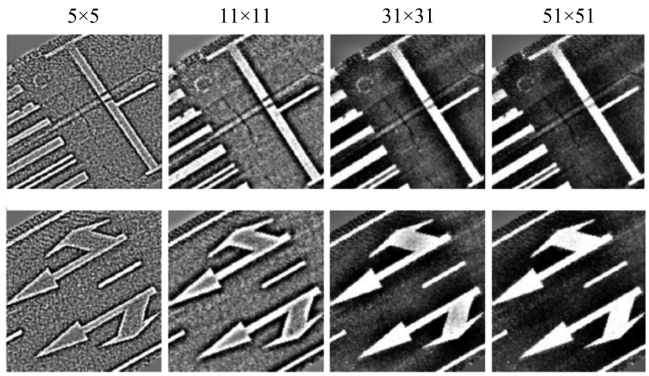

Fig. 14. High-pass results with different kernel sizes (from Sample02).

grid size of 5 cm, the thinnest road marking (line width 15 cm) can be presented in the intensity image, and the gaps between the MLS points will be interpolated. Therefore, the road surface points were rasterized by IDW with a grid size of 5 cm. Fig. 11(a) shows the intensity image generated by the IDW interpolation. In regard to intensity, the road markings look brighter than the pavements (asphalt). Nevertheless, the intensity of the pavement and the road markings are both unevenly distributed, which leads to large in-class variance.

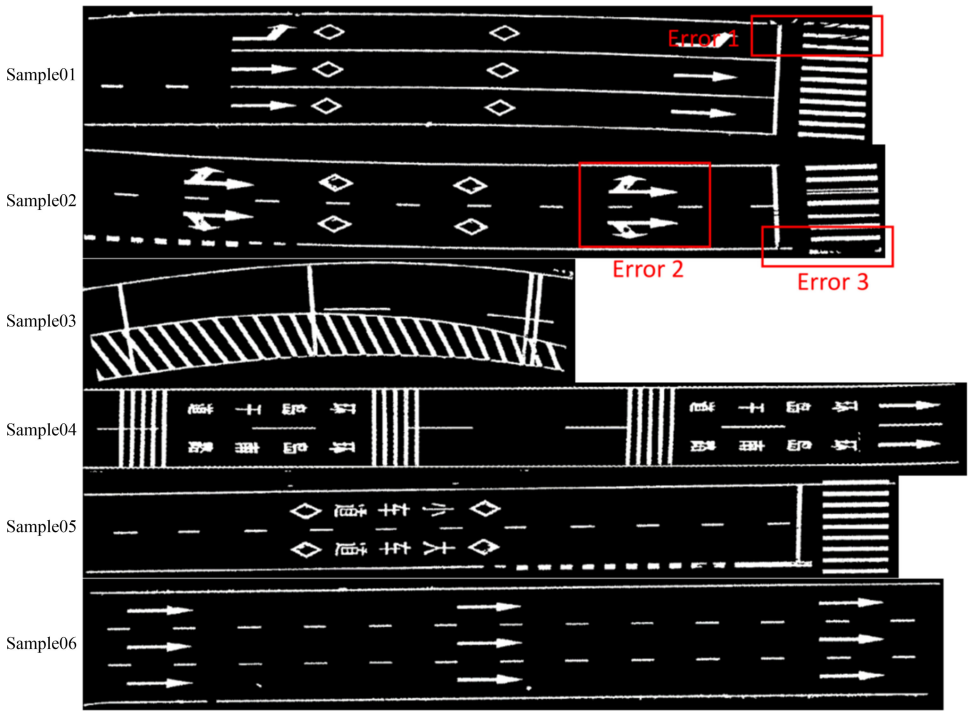

Fig. 15. Results of road-marking extraction.

TABLE I
QUANTITATIVE EVALUATION OF ROAD-MARKING EXTRACTION

Sample No.	01	02	03	04	05	06	07
Completeness	0.89	0.93	0.94	0.94	0.91	0.92	0.94
Correctness	0.96	0.94	0.96	0.96	0.98	0.95	0.92
F-score	0.93	0.93	0.95	0.95	0.94	0.94	0.93

A scan-angle-rank-based intensity correction was used to correct various intensity values caused by different incidence angles. The corrected intensity image is presented in Fig. 11(b). It is evident that the contrast between road markings and the pavements was enhanced; therefore, the road markings became more detectable. However, the variance of pavement intensity remained after the correction. The improvement of the intensity image is demonstrated in the histograms (see Fig. 12). It is clear that the distribution of the pavements and the road-marking intensity value are more concentrated by using the intensity correction process. The in-class variance of pavements and road markings decreases from 21.23 to 14.10 and 32.38 to 18.57, respectively. The difference between the road markings and the pavements also decreases from 91.10 to 78.42.

The intensity correction minimizes the in-class variance and keeps the interclass variance still; thus, the road markings become more detectable. The results indicate that the scan-angle-rank-based intensity correction works well on a global scale. Nonetheless, the intensity in some areas, which have different slopes and degrees of roughness, cannot be explained by the cosine of the scan angle rank. Therefore, a large-scale high-pass filtering approach was undertaken to eliminate the spatial variance caused by different degrees of pavement roughness.

The large-size high-pass kernel was designed to eliminate the slowly varying intensity components, and was validated using Sample02 and Sample06 to get the optimal size. The individual high-pass result is binarized by Otsu's thresholding method, and the extraction results are assessed by using manually labeled references. The performance of individual high-pass enhancement is represented by the *F*-score in an accuracy assessment. The *F*-score of results with different sizes of the high-pass kernel is shown in Fig. 13. The *F*-score increased sharply with size of the filter from 3×3 to 19×19. From 19×19 to 29×29, the *F*-score increased smoothly, and it reached the peak (93.66%) at 29×29. After that, the *F*-score of extraction decreased with increase of the filter size. In Fig. 14, the increase of the kernel size makes distinguishing the road markings from the pavement much easier. When the kernel size is bigger than 5×5 (25×25 cm^2), the thin road markings (15–20 cm) (e.g., boundary line, centerline, and traffic lane line) are detectable in the images. When the kernel size is bigger than 11×11 (55×55 cm^2), the road markings with medium width (40–45 cm) (e.g., stop line and a zebra crossing stripe) become detectable. When the kernel size exceeds 31×31 (155×155 cm^2), the widest road markings (e.g., road arrow) can be detected.

Theoretically, the larger the kernel size, the lower the cut-off frequency of the high-pass filter. If the kernel size is too large, the filter is not capable of removing the slowly varying intensity component. To strike a balance between detecting large road markings and eliminating spatial variance of intensity, the kernel size is set to 31×31. The high-pass-enhanced intensity image of Sample06 is shown in Fig. 11(c).

Fig. 16. Extracted road markings from Sample 05. From top to bottom: road surface point, Chen's result, Guan's result, Yu's result, result of proposed method, and manually labeled benchmark (adapted from [24]).

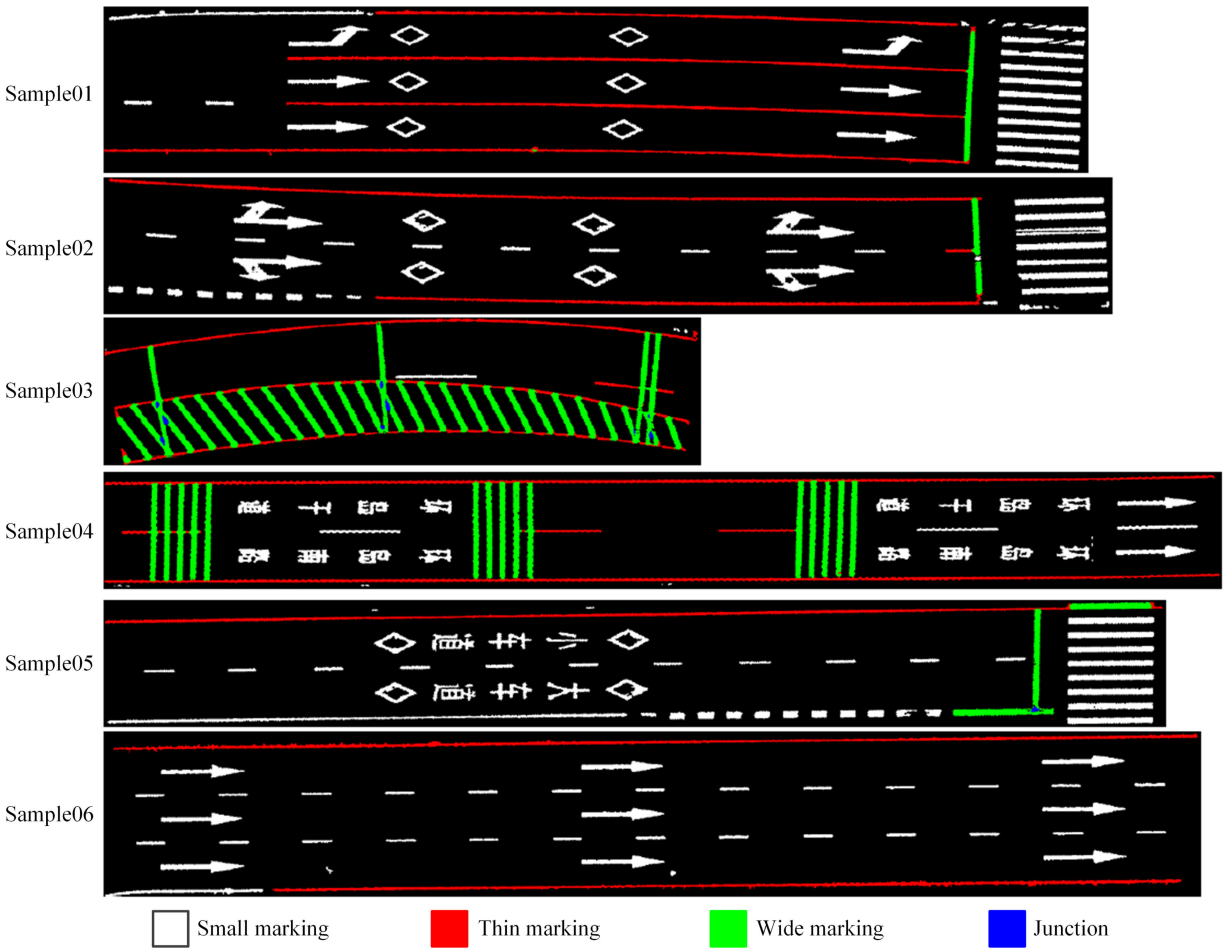

Fig. 17. Results of road-marking segmentation.

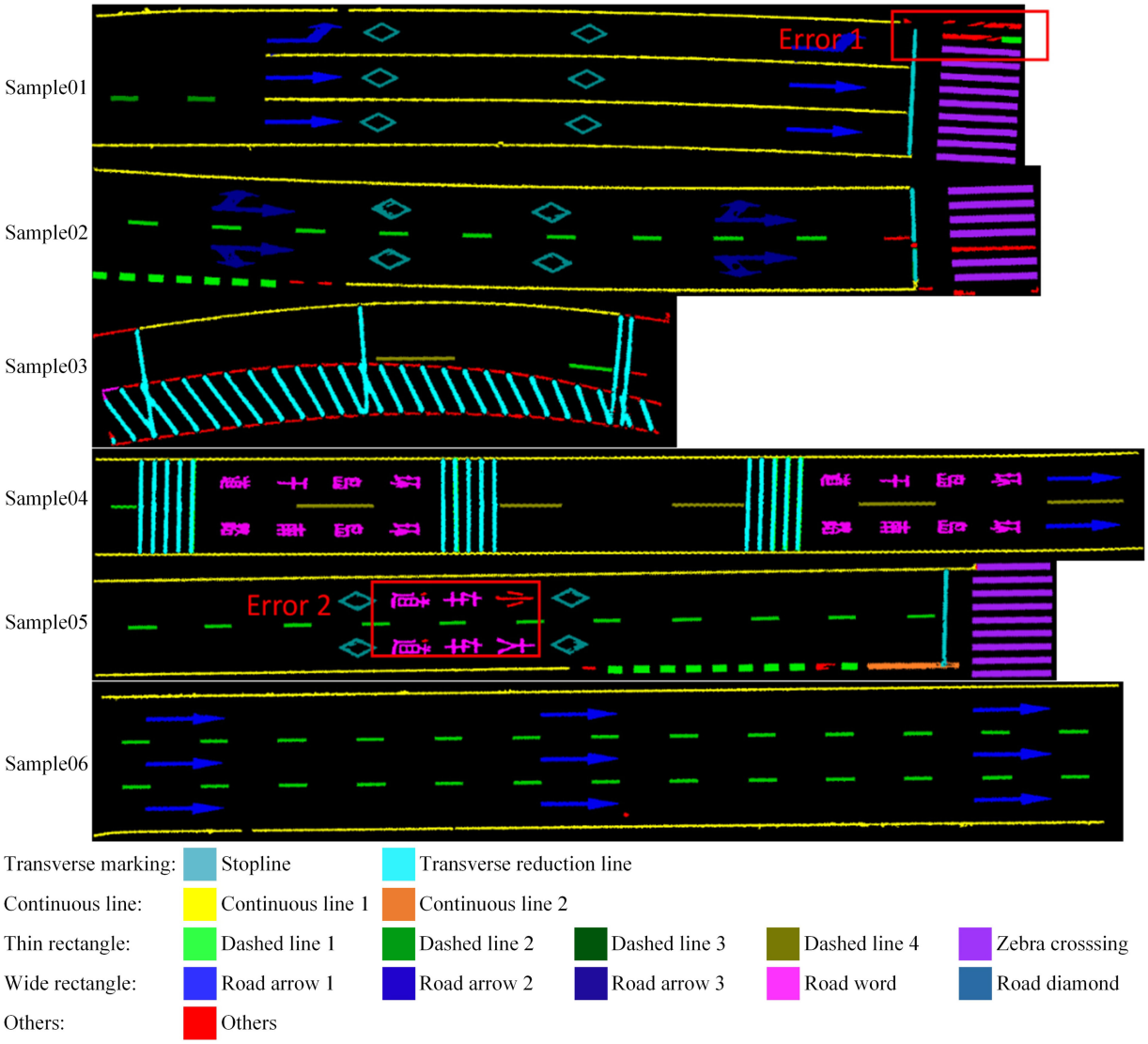

Fig. 18. Results of road-marking classification.

C. Road-Marking Extraction and Comparative Study

After the intensity correction and high-pass enhancement, the global Otsu's thresholding was implemented on the samples. The noises were removed from the extraction results by using 3 $\times$ 3 median filtering and the region growing method. As shown in Fig. 15, the majority of the road markings are extracted from the image but three incomplete markings. Errors 1 and 3 are caused by lack of sufficient laser points. The increase of the gaps between the laser points results in a low value that was interpolated into the intensity image. Error 2 is the false negative located in the inner of the road arrows caused by high-pass filtering.

The quantitative assessment of the results is listed in Table I; the proposed road-marking extraction is capable to achieve 0.92 completeness, 0.95 correctness, and 0.94 *F*-score on average. The rate of completeness is smaller than that of correctness in each sample, indicating that some marking pixels were misclassified into the pavements. Due to the decay of the road

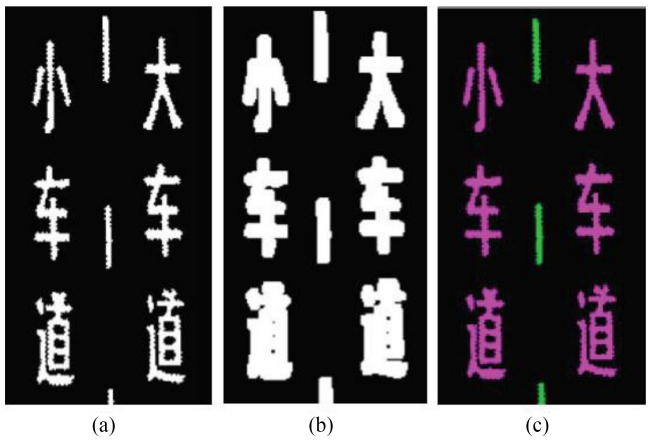

Fig. 19. Detection of Chinese characters: (a) road-marking region, (b) dilated road-marking region, and (c) Chinese characters classified in the dilated region.

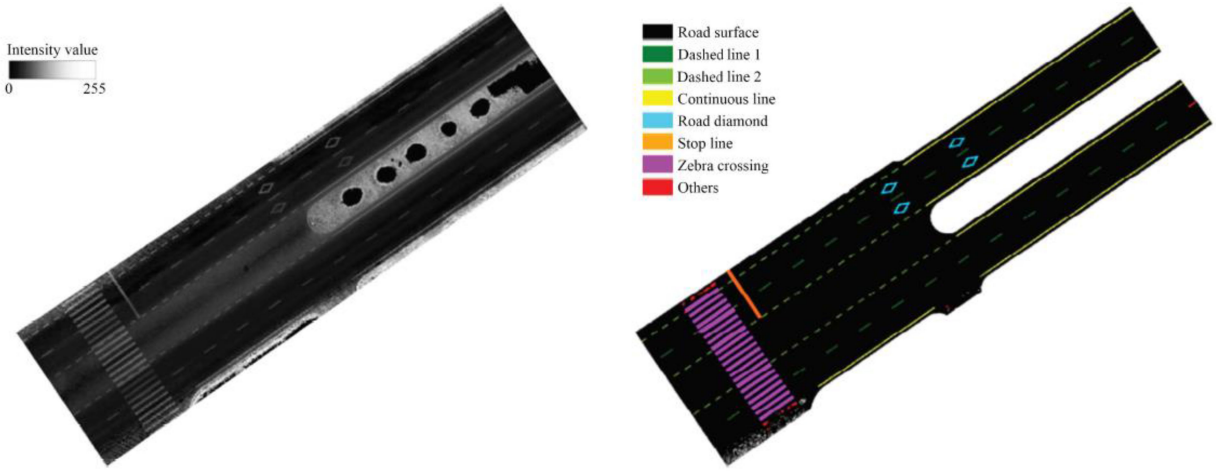

Fig. 20. (a) Road surface intensity image and (b) road-marking classification result of Sample07.

markings, the manually labeled references are bigger than the damaged road markings. Therefore, the performance of the proposed method was underestimated in the result.

A comparative study was carried out between the results from the proposed method and other studies including Chen's [21], Guan's [7], and Yu's [24] methods. The 2-D intensity image generated from point clouds was used in Guan's and the proposed methods for the extraction of road markings, whereas 3-D point clouds were directly applied in Chen's and Yu's studies. The evaluation results of these three methods are adapted from Yu's study, as shown in Fig. 16. One of the limitations in Chen's method is that the extraction focuses only on the lane markings along the traffic direction. Guan's, Yu's, and the proposed method have extended the extraction boundary to any types of road markings.

Compared with Guan's approach, an increased number of markings can be extracted using the proposed method. Based on the distribution of point density, Guan's method is capable to partition the road. However, Guan's method still suffered from the inconstant intensity, so that the road markings could not be distinguished from the rough pavement near the road boundary. It is also noted that Yu's method is point based, whereas Guan's and proposed method are pixel based. Therefore, Yu's method would not be affected by blurring data and achieves higher completeness.

The performance of these four methods is evaluated in a quantitative way, as shown in Table II. It is identified that the proposed method outmatches Chen's and Guan's methods but inferior to Yu's method in terms of the completeness.

TABLE II
QUANTITATIVE EVALUATION OF DIFFERENT ROAD-MARKING-EXTRACTION METHODS

Sample No.	01				05			
Method	Chen	Guan	Yu	Proposed	Chen	Guan	Yu	Proposed
Completeness	0.75	0.86	0.93	0.89	0.71	0.89	0.93	0.91
Correctness	0.91	0.90	0.92	0.96	0.92	0.91	0.91	0.98
F-score	0.82	0.88	0.93	0.93	0.80	0.90	0.92	0.94

D. Road-Marking Classification

Before the classification process, road markings were segmented into clusters by four-neighbor region growing. The segmentation results are presented in Fig. 17. Based on the neighbor counting filtering, the large regions of the road markings were segmented successfully, except in Sample03. The reserve area that was segmented into pieces cannot be interpreted correctly in Sample03.

The marking clusters were classified into categories based on the decision tree. All kinds of road markings in the samples are illustrated in Fig. 18. It is identified that the majority of the segments were classified into correct categories. Nevertheless, three problems arose in the classification.

Resulting from these three problems, there were a number of unclassified road-marking clusters within the images. In order to identify Chinese characters, successfully separating the strokes becomes crucial. One solution is to expand the clusters of strokes to generate a connected region, and then detect the strokes in one connect area as one character correctly. The dilation, as one of the basic operators in the area of mathematical morphology, was tested to connect separate strokes. Fig. 19 shows the dilation of Chinese characters and the recognition result. After region expanding, the strokes in one connect area can be classified as one character.

In order to solve the issue caused by the marking decay, a rectification method was employed to group the unclassified cluster to its nearest road marking. The basic idea is that these unclassified segments should be reclassified according to the confessedly recognized road-marking segments. Although the damaged road marking cannot be classified correctly by its geometric features, it still has a strong spatial relationship with its congeneric markings. Based on these correctly classified road-

marking segments, the near unclassified segment can be set into the closest road marking.

Since the proposed method is based on the global threshold strategy, it can process the multipath MLS data. The dataset in Xiamen was retrieved from a round-trip survey, and it consists of both back and forth point cloud data. Compared to the distance-dependent road-marking detection, the proposed method can process the entire dataset at one time without the trajectory data. The intensity image of the road surface and extraction results of Sample07 are shown in Fig. 20.

V. Conclusion

The majority of the existing MLS point cloud-based road-marking-extraction methods are based on the application of global intensity filtering and multithresholding segmentation. However, these methods could be greatly influenced by the unevenly distributed intensity. In this paper, we have proposed an effective method for solving the inconstant intensity issue. The method combines scan-angle-rank-based intensity correction and large-size high-pass filtering, and demonstrates potential to significantly reduce the in-class intensity variance of road markings and pavements. In addition, a shape-based hierarchical tree is developed to undertake the road-marking classification, which is based on the comprehensive prior knowledge and avoids the training process in machine learning based algorithms. A case study was undertaken to demonstrate the applicability of the proposed workflow. According to the results, the workflow is capable of accurate extraction and classification of the road markings in the MLS point clouds, and the average completeness, correctness, and F-score are 0.92, 0.95, and 0.94, respectively.

However, the efficiency of the intensity correction method depends on the flatness of the road surface. The cracking, rutting, and potholes, which are not in compliance with the plane model, can hardly be corrected by the proposed method. In the future, advanced radiometric calibration of MLS data should be developed and applied prior to the road-marking extraction. Furthermore, the decision tree for road-marking classification is shaped based and needs to be adjusted according to local traffic marking standards.

References

[1] E. Guizzo, How Google's self-driving car works, Oct. 2011. [Online]. Available: http://spectrum.ieee.org/automaton/robotics/artificial-intelligence/how-google-self-driving-car-works/

[2] L. Kent, Autonomous cars can only understand the real world through a map, Apr. 2015. [Online]. Available: http://360.here.com/2015/04/16/autonomous-cars-can-understand-real-world-map/

[3] I. Puente, H. González-Jorge, J. Martínez-Sánchez, and P. Arias, "Review of mobile mapping and surveying technologies," *Measurement*, vol. 46, no. 7, pp. 2127–2145, Aug. 2013.

[4] B. Yang and L. Fang, "Automated extraction of 3-D railway tracks from mobile laser scanning point clouds," *IEEE J. Sel. Topics Appl. Earth Observ. Remote Sens.*, vol. 7, no. 12, pp. 4750–4761, Dec. 2014.

[5] P. Kumar, P. Lewis, C. P. Mcelhinney, and P. Boguslawski, "Snake energy analysis and result validation for a mobile laser scanning data-based automated road edge extraction algorithm," *IEEE J. Sel. Topics Appl. Earth Observ. Remote Sens.*, 2016, to be published.

[6] B. Yang, L. Fang, and J. Li, "Semi-automated extraction and delineation of 3D roads of street scene from mobile laser scanning point clouds," *ISPRS J. Photogramm. Remote Sens.*, vol. 79, no. 5, pp. 80–93, May 2013.

[7] H. Guan, J. Li, Y. Yu, C. Wang, M. Chapman, and B. Yang, "Using mobile laser scanning data for automated extraction of road markings," *ISPRS J. Photogramm. Remote Sens.*, vol. 87, no. 1, pp. 93–107, Jan. 2014.

[8] Y. Zhou, D. Wang, X. Xie, and Y. Ren, "A fast and accurate segmentation method for ordered LiDAR point cloud of large-scale scenes," *IEEE Geosci. Remote Sens. Lett.*, vol. 11, no. 11, pp. 1981–1985, Nov. 2014.

[9] B. Wu, B. Yu, C. Huang, Q. Wu, and J. Wu, "Automated extraction of ground surface along urban roads from mobile laser scanning point clouds," *Remote Sens. Lett.*, vol. 7, no. 2, pp. 170–179, 2016.

[10] G. Vosselman, B. G. H. Gorte, G. Sithole, and T. Rabbani, "Recognizing structure in laser scanner point clouds," *Int. Arch. Photogramm., Remote Sens. Spatial Inf. Sci.*, vol. 36 (Part 8/W2), pp. 33–38, 2004.

[11] S. Pu, M. Rutzinger, G. Vosselman, and S. O. Elberink, "Recognizing basic structures from mobile laser scanning data for road inventory studies," *ISPRS J. Photogramm. Remote Sens.*, vol. 66, no. 6 (Supplement), pp. S28–S39, Dec. 2011.

[12] Y. Zhou, Y. Yu, G. Lu, and S. Du, "Super-segments based classification of 3D urban street scenes," *Int. J. Adv. Robot. Syst.*, vol. 9, pp. 14–18, 2012.

[13] A. Hervieu and B. Soheilian, "Semi-automatic road/pavement modeling using mobile laser scanning," *ISPRS Ann. Photogramm., Remote Sens. Spatial Inf. Sci.*, vol. II-3/W3, pp. 31–36, 2013.

[14] Z. Liu, J. Wang, and D. Liu, "A new curb detection method for unmanned ground vehicles using 2D sequential laser data," *Sensors*, vol. 13, no. 1, pp. 1102–1120, 2013.

[15] C. Cabo, C. Ordoñez, S. García-Cortés, and J. Martínez, "An algorithm for automatic detection of pole-like street furniture objects from mobile laser scanner point clouds," *ISPRS J. Photogramm. Remote Sens.*, vol. 87, no. 1, pp. 47–56, Jan. 2014.

[16] Y. Yu, J. Li, H. Guan, C. Wang, and J. Yu, "Semiautomated extraction of street light poles from mobile LiDAR point-clouds," *IEEE Trans. Geosci. Remote Sens.*, vol. 53, no. 3, pp. 1374–1386, Mar. 2015.

[17] L. Smadja, J. Ninot, and T. Gavrilovic, "Road extraction and environment interpretation from LiDAR sensors," *Int. Arch. Photogramm., Remote Sens. Spatial Inf. Sci.*, vol. 38 (Part 3A), pp. 281–286, 2010.

[18] C. Toth, E. Paska, and D. Brzezinska, "Using road pavement markings as ground control for LiDAR data," *Int. Arch. Photogramm., Remote Sens. Spatial Inf. Sci.*, vol. 37 (Part B1), pp. 189–196, 2008.

[19] B. Yang, L. Fang, Q. Li, and J. Li, "Automated extraction of road markings from mobile LiDAR point clouds," *Photogramm. Eng. Remote Sens.*, vol. 78, no. 4, pp. 331–338, Apr. 2012.

[20] A. Jaakkola, J. Hyyppä, H. Hyyppä, and A. Kukko, "Retrieval algorithms for road surface modelling using laser-based mobile mapping," *Sensors*, vol. 8, no. 9, pp. 5238–5249, 2008.

[21] X. Chen, B. Kohlmeyer, M. Stroila, N. Alwar, R. Wang, and J. Bach, "Next generation map making: Geo-referenced ground-level LiDAR point clouds for automatic retro-reflective road feature extraction," in *Proc. 17th ACM SIGSPATIAL Int. Conf. Adv. Geographic Inf. Syst.*, Seattle, WA USA, Nov. 4–6, 2009, pp. 488–491.

[22] G. Vosselman, "Advanced point cloud processing," in *Photogramm. Week*, Stuttgart, Germany, Sep. 7–11, 2009, pp. 137–146.

[23] P. Kumar, C. P. McElhinney, P. Lewis, and T. McCarthy, "Automated road markings extraction from mobile laser scanning data," *Int. J. Appl. Earth Observ. Geoinf.*, vol. 32, pp. 125–137, 2014.

[24] Y. Yu, J. Li, H. Guan, F. Jia, and C. Wang, "Learning hierarchical features for automated extraction of road markings from 3-D mobile LiDAR point clouds," *IEEE J. Sel. Topics Appl. Earth Observ. Remote Sens.*, vol. 8, no. 2, pp. 709–726, Feb. 2015.

[25] Q. Li, N. Zheng, and H. Cheng, "Springrobot: A prototype autonomous vehicle and its algorithms for lane detection," *IEEE Trans. Intell. Transp. Syst.*, vol. 5, no. 4, pp. 300–308, Dec. 2004.

[26] J. Rebut, A. Bensrhair, and G. Toulminet, "Image segmentation and pattern recognition for road marking analysis," in *IEEE Int. Symp. Ind. Electron.*, vol. 1, Ajaccio, France, May 4–7, 2004, pp. 727–732.

[27] A. Kheyrollahi and T. P. Breckon, "Automatic real-time road marking recognition using a feature driven approach," *Mach. Vis. Appl.*, vol. 23, no. 1, pp. 123–133, Jan. 2012.

[28] U. Franke, D. Gavrila, S. Görzig, F. Lindner, F. Paetzold, and C. Wöhler, "Autonomous driving goes downtown," *IEEE Intell. Syst.*, vol. 13, no. 6, pp. 40–48, Nov./Dec. 1998.

[29] P. Foucher, Y. Sebsadji, J.-P. Tarel, P. Charbonnier, and P. Nicolle, "Detection and recognition of urban road markings using images," in *Proc. 14th Int. IEEE Conf. Intell. Transp. Syst.*, Washington, DC, USA, Oct. 5–7, 2011, pp. 1747–1752.

[30] Y. Li, K. He, and P. Jia, "Road markers recognition based on shape information," in *Proc. IEEE Intell. Vehicles Symp.*, Istanbul, Turkey, Jun. 13–15, 2007, pp. 117–122.
[31] O. Tournaire, N. Paparoditis, and F. Lafarge, "Rectangular road marking detection with marked point processes," *Photogramm. Image Anal.*, vol. 36, no. 3, pp. 149–154, 2007.
[32] R. Danescu and S. Nedevschi, "Detection and classification of painted road objects for intersection assistance applications," in *Proc. 13th Int. IEEE Conf. Intell. Transp. Syst.*, Funchal, Portugal, Sep. 19–22, 2010, pp. 433–438.
[33] T. Wu and A. Ranganathan, "A practical system for road marking detection and recognition," in *Proc. IEEE Intell. Vehicles Symp.*, Alcalá de Henares, Spain, Jun. 3–7, 2012, pp. 25–30.
[34] N. Wang, W. Liu, C. Zhang, and H. Yuan, "The detection and recognition of arrow markings recognition based on monocular vision," in *Proc. Chin. Control Decision Conf.*, Guilin, China, Jun. 17–19, 2009, pp. 4380–4386.
[35] B. Mathibela, P. Newman, and I. Posner, "Reading the road: Road marking classification and interpretation," *IEEE Trans. Intell. Transp. Syst.*, vol. 16, no. 4, pp. 2072–2081, Aug. 2015.
[36] S. Kaasalainen, A. Jaakkola, M. Kaasalainen, A. Krooks, and A. Kukko, "Analysis of incidence angle and distance effects on terrestrial laser scanner intensity: Search for correction methods," *Remote Sens.*, vol. 3, no. 10, pp. 2207–2221, Oct. 2011.
[37] R. Adams and L. Bischof, "Seeded region growing," *IEEE Trans. Pattern Anal. Mach. Intell.*, vol. 16, no. 6, pp. 641–647, Jun. 1994.

Ming Cheng (M'14) received the Ph.D. degree in biomedical engineering from Tsinghua University, Beijing, China, in 2004.

He is currently an Associate Professor with both the Fujian Key Laboratory of Sensing and Computing for Smart Cities and Xiamen Key Laboratory of Geospatial Sensing and Computing, School of Information Science and Engineering, Xiamen University, Xiamen, China. His research interests include remote sensing image processing, point cloud processing, computer vision, and machine learning.

Dr. Cheng has published more than 30 papers in refereed journals and conference proceedings, including the IEEE GEOSCIENCE AND REMOTE SENSING LETTERS, *Neurocomputing*, and IGARSS and ISPRS proceedings.

Haocheng Zhang received the B.Sc. and M.Sc. degrees both in geomatics from the University of Waterloo, Waterloo, ON, Canada, in 2012 and 2015, respectively. The M.Sc. thesis was about rapid inspection of pavement markings using mobile laser scanning point clouds.

He is currently working as an Image Analyst with the Ecopia Tech, Waterloo, ON, Canada.

Cheng Wang (M'04–SM'16) received the Ph.D. degree in information and communication engineering from the National University of Defense Technology, Changsha, China, in 2002.

He is a Professor with the Fujian Key Laboratory of Sensing and Computing for Smart Cities and an Associate Dean of the School of Information Science and Technology, Xiamen University, Xiamen, China. His current research interests include remote sensing image processing, mobile LiDAR data analysis, and multisensor fusion.

Dr. Wang has coauthored about 150 papers published in refereed journals such as the IEEE TRANSACTIONS ON GEOSCIENCE AND REMOTE SENSING, IEEE TRANSACTIONS ON INTELLIGENT TRANSPORTATION SYSTEMS, IEEE GEOSCIENCE AND REMOTE SENSING LETTERS, IEEE JOURNAL OF SELECTED TOPICS IN APPLIED EARTH OBSERVATIONS AND REMOTE SENSING, and *ISPRS Journal of Photogrammetry and Remote Sensing* and conferences such as IGARSS and ISPRS. He is the Chair of the ISPRS Working Group I/6 on Multi-sensor Integration and Fusion (2016–2020). He is a Council Member of the Chinese Society of Image and Graphics.

Jonathan Li (M'00–SM'11) received the Ph.D. degree in geomatics engineering from the University of Cape Town, Cape Town, South Africa, in 2000.

He is currently a Professor with Fujian Key Laboratory of Sensing and Computing for Smart Cities, School of Information Science and Engineering, Xiamen University, Xiamen, China. He is also a Professor and the Head of the WatMos Lab, Faculty of Environment, University of Waterloo, Waterloo, ON, Canada. His current research interests include information extraction from LiDAR point clouds and from earth observation images.

Dr. Li has coauthored more than 300 publications, over 130 of which were published in refereed journals, including IEEE TRANSACTIONS ON GEOSCIENCE AND REMOTE SENSING, IEEE TRANSACTIONS ON INTELLIGENT TRANSPORTATION SYSTEMS (IEEE-TITS), IEEE GEOSCIENCE AND REMOTE SENSING LETTERS, IEEE JOURNAL OF SELECTED TOPICS IN APPLIED EARTH OBSERVATIONS AND REMOTE SENSING (IEEE-JSTARS), *ISPRS Journal of Photogrammetry and Remote Sensing*, *International Journal of Reliability and Safety*, *Photogrammetric Engineering & Remote Sensing*, and remote sensing of environment (RSE). He is the Chair of the ISPRS Working Group I/2 on LiDAR-, Air- and Spaceborne Optical Sensing (2016–2020), the Chair of the ICA Commission on Sensor-driven Mapping (2015–2019), and an Associate Editor of IEEE-TITS and IEEE-JSTARS.